Chinese Chemical Letters 37 (2026) 112111

Contents lists available at ScienceDirect

Chinese Chemical Letters

journal homepage: www.elsevier.com/locate/cclet

Shikonin ameliorates ulcerative colitis by inhibiting necroptosis *via* targeting HSPA8

Shuyu Wang[1], Yue Chai[1], Jinxin Shi[1], Pengcheng Dai, Ruizhi Yu, Hongming Shao, Wenxin Ding, Lijuan Xu, Runhui Liu*, Chunlin Zhuang*

The Center for Basic Research and Innovation of Medicine and Pharmacy (MOE), School of Pharmacy, Second Military Medical University, Shanghai 200433, China

ARTICLE INFO

Article history:
Received 25 October 2025
Revised 12 November 2025
Accepted 13 November 2025
Available online 13 November 2025

Keywords:
Ulcerative colitis
Shikonin
Necroptosis
HSPA8
Target

ABSTRACT

Ulcerative colitis (UC) is a pressing clinical issue currently lacking effective therapeutic approaches. Here we conducted a screening on the natural compounds from traditional Chinese medicine to identify a potent lead, shikonin (SHK), applying a necroptosis cell model. The potency for treating UC was confirmed in a dextran sulfate sodium (DSS)-induced UC mouse model. Leveraging a photo-affinity labeling approach, heat shock protein family A member 8 (HSPA8), a key negative regulator of necroptosis, was identified as the direct target of SHK. The *in vivo* protection of SHK were validated through targeting HSPA8 based on necroptosis pathway. As a result, targeting HSPA8 by SHK or activate HSPA8 significantly impairs necroptosis signaling and mitigates UC. Our findings not only define HSPA8 as a novel therapeutic target for UC but also highlight SHK as a promising lead for treatment of this symptom.

© 2026 Published by Elsevier B.V. on behalf of Chinese Chemical Society and Institute of Materia Medica, Chinese Academy of Medical Sciences.

Ulcerative colitis (UC), a major subtype of inflammatory bowel disease (IBD), is characterized by relapsing mucosal inflammation with an unclear etiology [1]. Due to the rising incidence and prevalence rates, UC has become a significant global health concern [2]. It is now recognized as a progressive disease, as it carries risks such as proximal extension, strictures, gut dysmotility, anorectal dysfunction, the need for colectomy, hospitalization, colorectal cancer, disability, and a diminished quality of life [1]. In 1955, corticosteroids were introduced to treat active inflammation in UC, leading to a significant reduction in the mortality rate among patients with moderate-to-severe UC [3]. However, their prolonged use is associated with significant adverse effects, such as osteoporosis, depression, moon face, type 2 diabetes mellitus, and cataracts [4]. Managing steroid-refractory patients especially those who are corticosteroid-dependent or -resistant remains a major clinical challenge [5].

The advanced biological therapies include targeting cytokines (*e.g.*, tumor necrosis factor-alpha (TNF-α), interleukin (IL)-12/23) and adhesion molecules (*e.g.*, $\alpha4\beta7$ integrin) [6]. However, these therapies are not universally effective: primary or secondary non-response occurs in a substantial subset of patients, and up to 20%–30% of individuals still require colectomy due to treatment failure or the development of dysplasia [7]. Besides, current research focuses on advancing precision medicine, such as using biomarkers to guide personalized therapy and developing novel agents (*e.g.*, JAK inhibitors, microbiome modulators, stem cell therapies) to address unmet needs in refractory disease [8]. Through these endeavors, the incidence rate has stabilized in Western countries, where the condition remains highly prevalent as a global health concern due to the increasing rates observed in developing nations [2]. This trend not only imposes a significant socioeconomic burden but also leads to a decline in patient well-being. Pathophysiologically, UC results from complex interactions among genetic predisposition, environmental triggers, immune dysregulation, and intestinal microbiota imbalance, with the precise molecular mechanisms still being actively investigated [1]. In recent years, necroptosis has emerged as a critical focus in UC pathogenesis research [9]. Necroptosis is a caspase-independent form of regulated cell death, dysregulated by its core signaling cascade, receptor-interacting protein kinases 1 and 3 (RIPK1/RIPK3) and mixed lineage kinase domain-like protein (MLKL) [10]. The intestinal epithelial cell (IEC) necroptosis disrupts mucosal barrier integrity, enhances inflammatory cell infiltration, and amplifies pro-inflammatory cytokine release, collectively exacerbating intestinal inflammation [11]. Pierdomenico *et al.* found necroptosis was active in children with IBD and contributed to strengthen the intestinal inflammatory process [12]. It was found that necroptosis was prevented by knocking out MLKL, in a dextran sulfate sodium (DSS) induced experimental col-

* Corresponding authors.
E-mail addresses: lyliurh@126.com (R. Liu), zclnathan@163.com (C. Zhuang).
[1] These authors contributed equally to this work.

https://doi.org/10.1016/j.cclet.2025.112111
1001-8417/© 2026 Published by Elsevier B.V. on behalf of Chinese Chemical Society and Institute of Materia Medica, Chinese Academy of Medical Sciences.

itis [13]. Inhibiting necroptosis by chemicals significantly alleviated DSS-induced colitis *in vivo*, cell death and inflammatory response [14]. Thus, inhibiting excessive necroptosis may represent a promising therapeutic approach for UC. Nevertheless, the function of genes with abnormal regulation that drive necroptosis in UC remains largely uninvestigated.

To further delineate the necroptosis signaling and identify novel therapeutic agents of UC, we assembled a structurally diverse natural compounds from traditional Chinese medicine (TCM) and evaluated the anti-necroptosis potential through screening. Shikonin (SHK), a principal bioactive constituent of *Lithospermum erythrorhizon* root extract, was identified as an active compound against necroptosis. It had a long-standing application in traditional medicine, including anti-tumor, anti-inflammatory, immunomodulatory, and wound-healing activities [15]. We first demonstrate here that SHK is a potent necroptosis inhibitor, investigating the potency in a DSS-induced UC mouse model. For mechanism, SHK exerts its protective effects by directly targeting heat shock protein family A member 8 (HSPA8), a key negative regulator of necroptosis, and enhanced the ATPase activity of HSPA8. SHK treatment could enhance HSPA8′s fibril disassembly activity. The *in vivo* protection of SHK were validated through targeting HSPA8 based on necroptosis pathway. Our work suggests that HSPA8 is a novel therapeutic target in necroptosis-mediating UC pathway, and SHK is a promising anti-UC lead compound for treating necroptosis-associated diseases.

We first generated a necroptosis model through TNF-α, Smac mimetic SM-164, and pan-caspase inhibitor z-VAD-FMK (TSZ) stimulation in human HT-29 cells [16]. A structurally diverse natural compounds from TCM was screened was screened for their ability to block the necroptosis at a concentration of 10 μmol/L (Fig. 1A and Table S1 in Supporting information). Among them, a naphthoquinone compound, SHK, was found to clearly protect HT-29 cells from TSZ-induced necroptosis with a cell viability higher than 90%. A dose-response assay quantitatively determined the inhibitory potency of SHK with a half-maximal effective concentration (EC_{50}) value of 2.6 ± 0.21 μmol/L (Fig. 1B). It also effectively inhibited necroptosis induced by TNF-α, cycloheximide, and z-VAD-FMK (TCZ, Fig. S1A in Supporting information). In human Eol-1 cells and U937 cells, SHK could almost reverse TSZ-induced necroptosis at a concentration of 5 μmol/L (>90%, Fig. 1C). We found that SHK dose-dependently protected from TNF-α and z-VAD-FMK (TZ)-induced necroptosis at a concentration of 10 μmol/L in murine L929 cells (Fig. 1D) and necroptosis induced by lipopolysaccharide and z-VAD-FMK (LZ) at 3.125 μmol/L in murine RAW264.7 cells (Fig. S1B in Supporting information). Remarkably, SHK did not protect cells from TNF-α plus Smac mimetic (TS) or cycloheximide (TC)-induced apoptosis in HT-29 cells, suggesting that SHK specifically inhibited the necroptosis pathway (Figs. S1C and D in Supporting information). The entire process of necroptosis in HT-29 and L929 cells with or without SHK was recorded by a live-cell super-resolution panoramic microscopy (Fig. 1E and Supplemental movies for Fig. 1D in Supporting information). In HT-29 cells, the cell morphology became round at 4 h after TSZ-induced necroptosis, followed by swelling and membrane rupture. After 6 h, all the cells died. Differently, there was no significant change in cell morphology with the treatment of SHK, and all cells survived at 6 h after TSZ induced necroptosis. Similar changes were observed in L929 cells after TZ-induced necroptosis with or without SHK, which resulted in cell death within 5 h. Concurrently, following the treatment of SHK, the cellular morphology exhibited a rounded shape without inducing cell death, indicating an obvious protective effect. Our findings indicate that SHK is a potential inhibitor specially toward necroptosis rather than apoptosis.

Necroptosis in systemic inflammatory response syndrome (SIRS) has been well-documented [17]. The TZ-induced SIRS model triggers severe inflammatory storms in mice, ultimately resulting in hypothermia and mortality. All animal experiments were undertaken in accordance with the National Institute of Health Guide for the Care and Use of Laboratory Animals, with the approval of the Animal Care and Use Committee of Naval Medical University, Shanghai, China. In this model, mice were firstly peritoneally injected (i.p.) with z-VAD-FMK, and then intravenously injected (i.v.) with TNF-α, and SHK at doses of 1.25, 2.5, or 5 mg/kg was given by orally administration 2 h before TNF-α. We observed that the body temperature of model mice dropped sharply to below 24 °C within 10 h. In contrast, mice treated with SHK were significantly protected from TNF-induced hypothermia and death (Fig. 1F). Survival analysis revealed that there was 100% mortality in model mice, while the survival rates were 16.7% (low dose), 58.3% (medium dose), and 91.7% (high dose) in mice treated with SHK ($n = 12$/group, $P < 0.001$). The decrease in body temperature caused by SIRS was significantly improved with SHK treatment (Fig. 1G). The pro-inflammatory factors IL-1β and IL-6 in serum and different organs were detected. IL-1β levels in lung, spleen, kidney, and intestine were elevated in the model group, and significantly reduced in the SHK-treated group (high dose). IL-1β levels in serum, heart, and brain were not significantly altered in both groups (Fig. 1H). IL-6 levels in serum and tissues were significantly higher in the model group than in controls, whereas SHK treatment signifi-

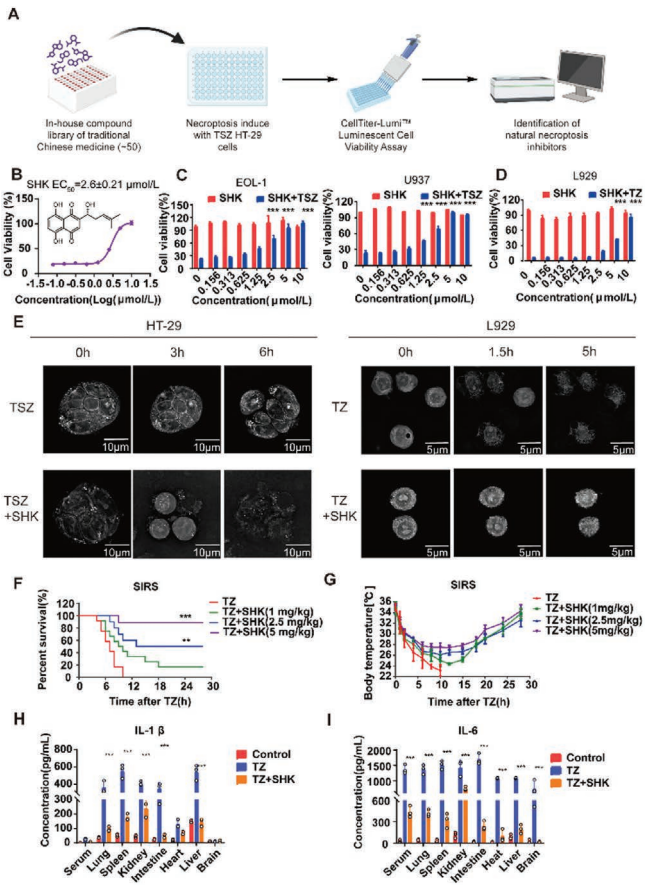


Fig. 1. SHK specifically inhibited necroptosis. (A) Schematic overview of Chinese medicine monomer screen workflow. (B) Structure and protective effects of SHK on TSZ models in HT-29 cells ($n = 3$). (C) Protective effects of SHK on TSZ models in EOL-1 and U937 cells. (D) Protective effect of SHK on TZ model in L929 cells. (E) A live-cell imaging (MH−HoliView, Cheng Guan Optical Technology (Nantong) Co., Ltd., China) of HT-29 cells treated with TSZ, TSZ+SHK (8 μmol/L) and L929 cells treated with TZ, TZ+ SHK (8 μmol/L). Scale bar: 10 μm (left), 5 μm (right). (F) Survival rates of SIRS models ($n = 12$). (G) Body temperature of mice in SIRS models ($n = 12$). (H, I) Serum and tissue IL-1β and IL-6 concentrations ($n = 3$). $^{**}P < 0.01$, $^{***}P < 0.001$ *vs.* TZ. Data are presented as mean ± standard error of the mean (SEM).

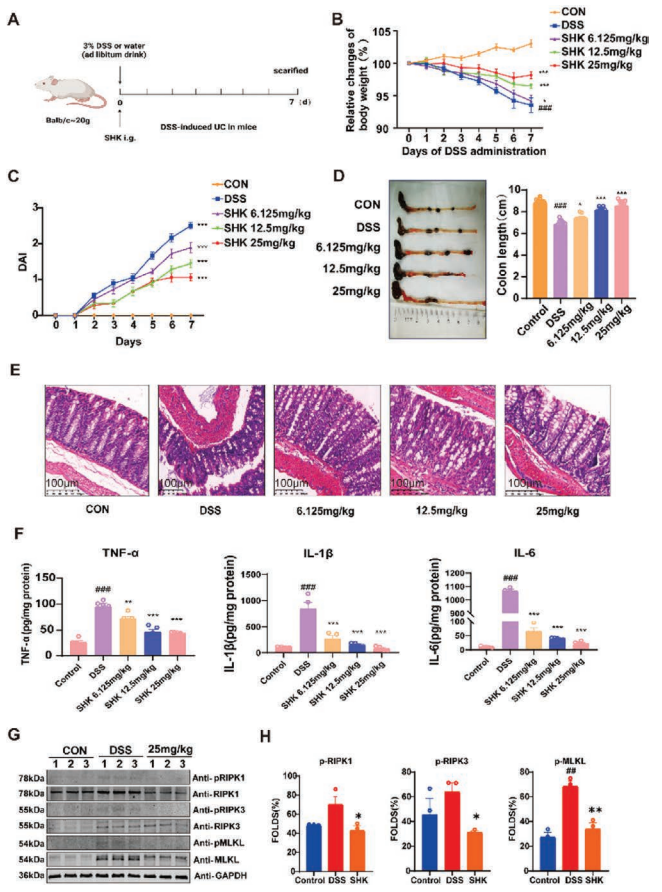


Fig. 2. SHK protects mice from DSS-induced UC. (A) Schematic overview of DSS-induced UC and the intervention of SHK. (B, C) Effect of SHK on body weight and DAI of mice ($n = 12$). (D) Effect of SHK on colon length of mice ($n = 12$). (E) Effect of SHK on the pathomorphology of colon of mice (200×). Scale bar: 100 μm. (F) Colon tissue TNF-α, IL-1β and IL-6 concentrations ($n = 5$). (G, H) Immunoblotting of pathway proteins in mice colonic tissue; and grey scale analysis of necroptosis pathway proteins ($n = 3$). $^{*}P < 0.05$, $^{**}P < 0.01$, $^{***}P < 0.001$ *vs.* DSS; $^{\#\#}P < 0.01$, $^{\#\#\#}P < 0.001$ *vs.* control (CON). GAPDH, glyceraldehyde-3-phosphate dehydrogenase. Data are presented as mean ± SEM.

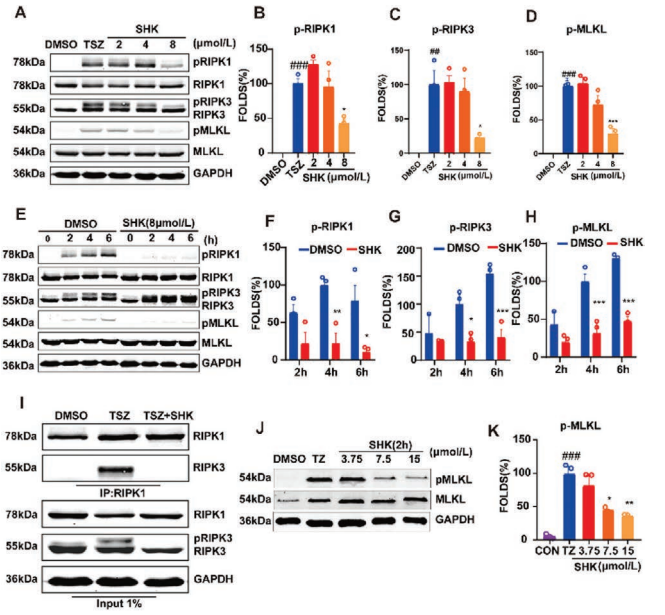


Fig. 3. SHK blocks necrosome formation. (A) Immunoblotting of TSZ model pathway proteins in HT-29 cells under different concentrations of SHK treatment. (B-D) Grey scale analysis of RIPK1, RIPK3 and MLKL phosphorylation statistics ($n = 3$). (E) Immunoblotting of pathway proteins at different time periods in the TSZ model of HT-29 cells after DMSO and SHK treatment ($n = 3$). (F–H) Grey scale analysis of p-RIPK1, p-RIPK3 and p-MLKL phosphorylation statistics ($n = 3$). (I) Interaction between RIPK1 and RIPK3 was detected by co-immunoprecipitation and immunoblotting in cultured HT-29 cells with indicated treatments. (J) Immunoblotting of MLKL in the TZ model of L929 cells under different concentrations of SHK treatment. (K) Grey scale analysis of MLKL phosphorylation statistics ($n = 3$). $^{\#\#}P < 0.01$, $^{\#\#\#}P < 0.001$ *vs.* DMSO; $^{*}P < 0.05$, $^{**}P < 0.01$, $^{***}P < 0.001$ *vs.* TSZ. Data are presented as mean ± SEM.

cantly attenuated IL-6 elevation in both serum and tissues (Fig. 1I). In summary, SHK is capable of effectively suppressing the inflammatory storm induced by SIRS.

Subsequently, we evaluated the anti-inflammatory efficacy of SHK in DSS-induced UC model [18,19], a condition that is distinctly linked to necroptosis. Except for the control group, all mice were administered 3 % DSS in drinking water for 7 days to induce UC. SHK treatment groups received oral gavage of SHK solutions at different concentrations (0.1 mL/10 g body weight daily), for a period of 7 days (Fig. 2A). DSS-treated mice developed progressive weight loss starting on day 3 (Fig. 2B), accompanied by diarrhea, hematochezia, and coat color alterations. SHK administration significantly mitigated weight loss in a dose-dependent manner. Disease activity index (DAI) was then utilized to quantitatively assess body weight reduction, stool consistency, and occult blood in UC mice. Compared with vehicle-treated controls, SHK treatment led to a more rapid dose-dependent reduction in DAI scores (Fig. 2C). In addition, mice administered SHK exhibited significantly longer colon lengths compared to vehicle-treated colitis controls (Fig. 2D). Histopathological analysis revealed that SHK treatment dose-dependently attenuated ulceration, mucosal epithelial loss, goblet cell depletion, and inflammatory cell infiltration in colonic tissues (Fig. 2E).

Enzyme-linked immunosorbent assay (ELISA) analysis revealed that the expression of pro-inflammatory cytokines TNF-α, IL-1β, and IL-6 was significantly upregulated in colon tissue homogenates of DSS-induced colitis mice (Fig. 2F). SHK treatment dose-dependently reduced the levels of these cytokines, effectively inhibiting inflammatory progression. These results demonstrate that SHK alleviates colonic inflammation in UC by downregulating TNF-α, IL-1β, and IL-6 expression. Western blot analysis revealed significantly upregulated expression of RIPK3 and MLKL in DSS-induced colitis mice compared to vehicle-treated controls, with marked increases in phosphorylated p-RIPK1, p-RIPK3, and p-MLKL. Phosphorylation of all three proteins was potently attenuated in mice treated with 25 mg/kg SHK (Figs. 2G and H).

In the TSZ model of HT-29 cells, we examined the impact of SHK on necroptotic pathway proteins across different time periods and found that it was able to inhibit the phosphorylation process of RIPK1 (S166), RIPK3 (S227), and MLKL (S358). SHK significantly suppressed the activation and phosphorylation of RIPK1, RIPK3, and MLKL at 8 μmol/L, with a clear dose-dependent pattern on MLKL phosphorylation (Figs. 3A–D). In a time-course experiment (2–6 h treatment window), SHK at 8 μmol/L significantly attenuated RIPK1 phosphorylation at 6 h, followed by subsequent reduction in both RIPK3 and MLKL phosphorylation compared to the control group (Figs. 3E–H). These results indicated that SHK was able to inhibit the activation of necroptosis-related proteins, thus we believe that SHK can interfere with the formation of necrosome. Immunoprecipitation analysis revealed that SHK potently blocked TSZ-induced the interaction between RIPK1 and RIPK3 at 8 μmol/L (Fig. 3I). In summary, our findings demonstrate that SHK exerts its function by affecting the formation of necrosome.

Next, to verify the effect of SHK on the necroptosis signaling pathway in mouse cells, we employed the L929 cell TZ model. The results revealed that it significantly inhibited MLKL phosphorylation in a concentration-dependent manner. Specifically, when the

concentration reached 15 μmol/L, SHK could markedly suppress MLKL protein phosphorylation (Figs. 3J and K). However, the binding targets of SHK for the anti-necroptosis still unclear. Applying SHK as a tool compound, we may potentially find novel targets for necroptosis.

SHK is an active component isolated from *Lithospermum erythrorhizon* roots. Previous studies reported its extensive biological activity [20,21]. It is the first time to find its anti-necroptosis activity, encouraging us to identify the molecular targets and relevant mechanisms. Activity-based protein profiling (ABPP) using photolabeling approach is an attractive and effective method for identifying the binding targets of natural products [22,23]. We first developed a clickable photolabeling tag on the potential position of the SHK scaffold. This tag enables a candidate to covalently capture proteins at specific residues following *in-situ* photo-crosslinking in biological systems, providing more reliable binding information for analyzing the target [24]. Before introducing the tag, we first compared the activity of SHK with a *R*-1-OH group and the derivatives with a *S*-1-OH, or without 1-OH (Fig. 4A). These compounds exhibited comparable activities, suggesting chemical modification tolerance on this position. Consequently, we generated a probe by modifying the 1-OH group of SHK with a diazirine alkyne tag (SHK-11). The chemical structure of SHK-11 was fully characterized by ^{1}H nuclear magnetic resonance spectroscopy (NMR), ^{13}C NMR spectroscopy, and high-resolution mass spectrometry (HRMS). The anti-necroptosis test demonstrated the probe still conserved a decent dose-dependently protective activity in a range of 5–20 μmol/L in human HT-29 cells (Fig. 4B), as well as in murine L929 cells (Fig. 4C).

We next performed the labeling experiments using HT-29 cells. After photo-crosslinking by exposed to UV radiation at 365 nm, the cell lysates were prepared and followed by being subjected to a click chemistry reaction with Biotin-PEG_3-N_3 and Cu(I)-catalyzed azide-alkyne cycloaddition (CuAAC). Then, the probe-captured proteins were pulled down, followed by sodium dodecyl sulfate-polyacrylamide gel electrophoresis (SDS-PAGE) (Fig. 4D). The bands at ~50–90 and 33–43 kDa were prominently labeled by the probe, which could be apparently competed with excessive SHK, suggesting likely binding targets (Fig. S2A in Supporting information). Next, we tried similar procedures using *in situ* cells or *in vitro* lysis. Proteins labeled by SHK-11 were enriched using streptavidin-conjugated magnetic beads and similar bands were found (Fig. 4E). Next, the entire band was digested and then underwent liquid chromatography tandem-mass spectrometry (LC-MS/MS) analysis. The MS data were analyzed by taking the intersection based on DMSO, SHK-11 *in situ* and *in vitro*. Venn diagram of the MS data was generated (Fig. 4F). Among the resulting 7 proteins, only 1 hit was obtained with the criteria of and MW (50–90 and 33–43 kDa), peptide (PEP) score (>20), unique peptides mapped (>3). HSPA8, a member of the heat shock protein 70 (HSP70) family, is a heat shock homologous protein with molecular weight of 70.9 kDa, and 4 unique peptides were identified and a PEP score of 4.936 for HSPA8.

Then, the cellular thermal shift assay (CETSA) [25] and drug affinity responsive target stability (DARTS) [26] were conducted to determine the target engagement of SHK in HT-29 cells. CETSA demonstrated that SHK significantly increased HSPA8 thermal stability (Figs. 4G and H). The results of the *in-situ* incubation of cells were consistent with the above results (Figs. S2B and C in Supporting information). DARTS reflected that SHK enhanced proteolytic resistance of HSPA8 in the treated cells (Figs. 4I and J). What is more, a streptavidin-based pull-down assay confirmed that HSPA8 was specifically enriched by SHK-11 and competitively displaced by excess SHK (Fig. 4K). These findings strongly suggest HSPA8 as a target protein of SHK in necroptosis. Next, we asked how SHK binds HSPA8. A bio-layer interferometry (BLI) analysis directly

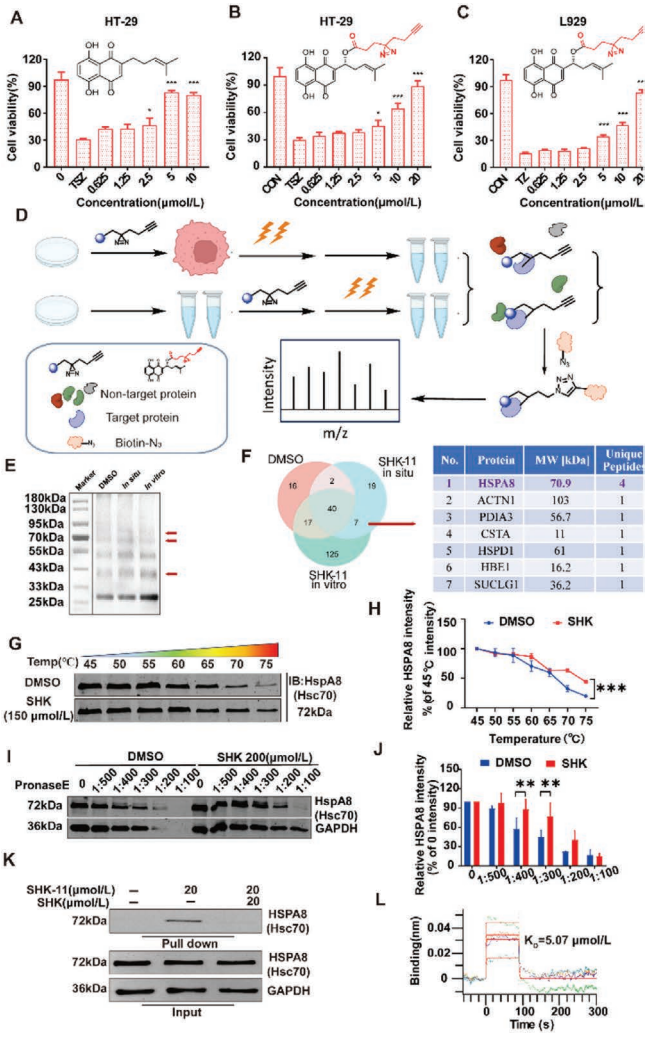


Fig. 4. Target identification of SHK in HT-29 cells by an ABPP strategy. (A–C) Anti-necroptosis effects of SHK and SHK-11 ($n = 3$). $^{*}P < 0.05$, $^{***}P < 0.001$ *vs.* TSZ/TZ. (D) Schematic illustration of target protein capture of SHK-11 in HT-29 based on ABPP. (E) SDS-PAGE image of SHK-11 enriched proteins. (F) Venn diagram of proteins enriched by photoaffinity probe SHK-11 in HT-29, and the possible target proteins were shown in the right table. (G, H) Immunoblotting of HSPA8 at different temperature after DMSO and SHK treatment in lysis and grey scale analysis of HSPA8 statistics ($n = 3$). $^{***}P < 0.001$. (I, J) Immunoblotting of HSPA8 at different dose pronase E after DMSO and SHK treatment and grey scale analysis of HSPA8 statistics ($n = 3$). $^{**}P < 0.01$. (K) Pull-down analysis of SHK-binding to HSPA8 in HT-29 cells. (L) A representative plot of the BLI signal against time. Data are presented as mean ± SEM.

quantified SHK-HSPA8 binding with a dissociation constant (K_D) of 5.09 μmol/L (Fig. 4L).

We next detected the effects on the protein expression of HSPA8 after the treatment of SHK (Fig. 5A). The results of immunofluorescence intensity analysis in HT-29 cells showed that TSZ-induced necroptosis led to downregulated HSPA8 expression, which could be restored by treatment with 8 μmol/L SHK. Consistent results were observed in animal models: in the DSS-induced model group, HSPA8 expression was decreased, and administration of 25 mg/kg SHK restored HSPA8 levels (Fig. S2I in Supporting information). Additionally, immunofluorescence in HT-29 cells revealed that SHK not only restored HSPA8 expression but also increased its cytoplasmic accumulation and colocalization with p-RIPK3 under TSZ-activated necroptosis (Fig. 5A). To validate the role of HSPA8 in HT-29 cell necroptosis, we designed and constructed a pLKD.1-shHSPA8-copGFP-Puro lentiviral plasmid. Knock-

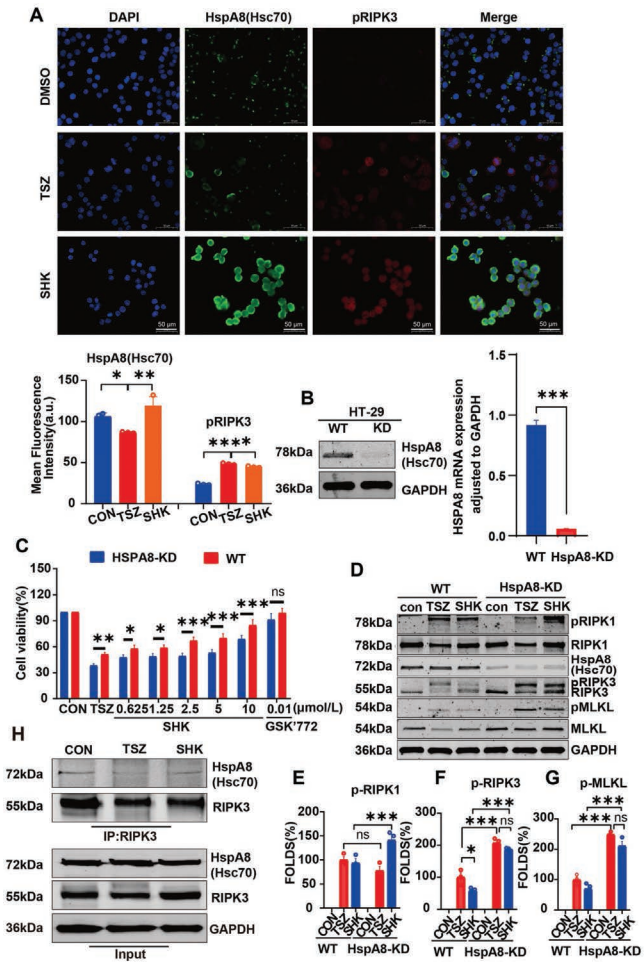


Fig. 5. SHK inhibits necroptosis dependent on HSPA8. (A) Immunofluorescence assay of the colocation of HspA8 and pRIPK3 in TSZ-induced HT-29 cells treated with SHK (8 μmol/L) or vehicle (DMSO). Scale bar: 50 μm. (B) The protein and mRNA levels of HSPA8 in HSPA8-KD cells. (C) Anti-necroptotic activity of SHK in HSPA8-KD cells ($n = 3$). (D) Immunoblotting of TSZ model pathway proteins by SHK in HSPA8-KD cells. (E–G) Grey scale analysis of statistics ($n = 3$). (H) Interaction between HSPA8 and RIPK3 was detected by co-immunoprecipitation and immunoblotting in cultured HT-29 cells with indicated treatments. $^{*}P < 0.05$, $^{**}P < 0.01$, $^{***}P < 0.001$. ns, no significance; DAPI, 4′,6-diamidino-2-phenylindole; WT, wild type. Data are presented as mean ± SEM.

down (KD) efficacy was confirmed by immunoblotting using anti-HSPA8 antibody and RT-qPCR analysis, demonstrating significant reduction of HSPA8 protein and mRNA levels (Fig. 5B). Cell viability assays revealed that HSPA8-KD in HT-29 cells significantly exacerbated TSZ-induced necroptosis (Fig. 5C). Notably, the ability of SHK to rescue cell viability was reduced in HSPA8-KD HT-29 cells compared to control knockdown cells (Fig. 5C), but not for a classical RIPK1-targeting compound GSK-772, confirming that SHK-mediated necroptosis inhibition is dependent on HSPA8. The results suggest that endogenous HSPA8 negatively regulates necroptosis.

The Western blot results were consistent with the findings from the activity assay (Figs. 5D–G). Under identical TSZ induction conditions, the phosphorylation levels of necrotic pathway proteins RIPK1, RIPK3, and MLKL were elevated in HSPA8-KD HT-29 cells. Meanwhile, the inhibitory effect of SHK on their phosphorylation was significantly attenuated, which was consistent with the results observed upon application of the HSPA8 inhibitor (Figs. S2D–H in Supporting information). These data indicate that HSPA8 knockdown impairs the ability of SHK to suppress necroptosis in the TSZ-induced HT-29 cell model. Moreover, immunoprecipitation experiments demonstrated direct interaction between HSPA8 and RIPK3 in HT-29 cells, and SHK promoted this interaction under TSZ-activated necroptosis (Fig. 5H). Collectively, these data indicate that SHK exerts its anti-necroptosis effect through HSPA8.

Herein, we report for the first time that SHK inhibits TSZ-induced necroptosis in HT-29 cells and ameliorates SIRS and DSS-induced UC in mice. Using activity-based protein profiling (ABPP), we identified HSPA8 as the direct cellular target mediating SHK's anti-necroptotic activity. HSPA8 is known to inhibit necroptosis by regulating RIP homotypic interaction motif (RHIM) domain polymerization and depolymerization of RHIM-containing protein fibers. We further demonstrated that SHK enhances HSPA8 binding to RIPK3 polyfibers and promotes their disassembly in TSZ-activated HT-29 cells. Collectively, these findings provide novel mechanistic insight into SHK's dual role in inhibiting necroptosis and inflammation *via* the HSPA8-RIPK3 axis, while establishing this natural product as a promising therapeutic lead for inflammatory disorders, including UC [27,28].

Numerous studies have focused on the anti-inflammatory activity of SHK, demonstrating that this compound can regulate inflammatory responses through multi-target, multi-pathway mechanisms and holds great potential for treating neuroinflammatory, digestive, cutaneous, and autoimmune inflammatory diseases [29,30]. SHK was shown to reduce the production of pro-inflammatory cytokines in colonic tissue, repair the intestinal barrier, mitigate intestinal histopathological damage, and alleviate intestinal inflammation by regulating signaling pathways such as nuclear factor kappa B (NF-κB), janus kinase/signal transducer and activator of transcription 3 (JAK/STAT3), and phosphoinositide 3-kinase/protein kinase B (PI3K/AKT) [31]. Our current screening reveals an anti-necroptotic activity of SHK. It is likely associated with multi-target pharmacological effects of SHK and the crosstalk between pathways. Varying experimental conditions, such as drug concentration, treatment duration, cell type, and inducer type, can lead to divergent outcomes, highlighting the scientific value of investigating the complex pharmacology of SHK.

In this study, we characterized the anti-necroptotic activity of SHK in a TSZ-induced HT-29 cell necroptosis model, identified potential molecular targets, and demonstrated that SHK suppresses necroptosis to attenuate the onset and progression of UC. These results indicate that SHK exerts therapeutic effects in UC by modulating multiple inflammatory signaling axes, positioning it as a promising candidate for novel UC therapies. Beyond expanding the known anti-inflammatory mechanisms of SHK, these findings provide robust pharmacological evidence to support its clinical translation, particularly in leveraging TCM principles for precision inflammatory disease management.

HSPA8 serves as a critical negative regulator of necroptosis [32]. Recent studies reveal that HSPA8 specifically recognizes RIP homotypic interaction motif (RHIM)-containing proteins (*e.g.*, RIPK1, RIPK3) and disrupts their amyloid-like fibril formation [32,33]. This mechanistic insight not only advances our understanding of cell death regulation but also establishes HSPA8 as a druggable target for inflammatory diseases. Therefore, regulation of necroptosis by targeting HSPA8 may be used to treat IBD, sepsis and other inflammatory diseases. In addition, the fiber depolymerization mechanism of HSPA8 also provides new ideas for the treatment of cancer and neurodegenerative diseases. Although our findings show that SHK inhibits necroptosis by modulating HSPA8 activity, the precise molecular mechanism, whether *via* direct regulation of HSPA8-ATP/ADP binding or alteration of its co-chaperone interaction affinity, remains unclear. Specifically, whether SHK enhances nucleotide exchange kinetics or disrupts chaperone complex formation to exert anti-necroptotic effects requires further investigation. These hypotheses require validation through biochemical assays and structural biology approaches, which will clarify whether SHK acts as

an allosteric activator or competitive inhibitor of HSPA8's chaperone function in necroptotic signaling.

CRediT authorship contribution statement

Shuyu Wang: Writing – original draft, Methodology, Investigation. **Yue Chai:** Writing – original draft, Methodology, Investigation. **Jinxin Shi:** Writing – original draft, Investigation. **Pengcheng Dai:** Methodology, Investigation. **Ruizhi Yu:** Investigation. **Hongming Shao:** Methodology, Investigation. **Wenxin Ding:** Validation, Methodology, Investigation. **Lijuan Xu:** Validation, Methodology, Investigation. **Runhui Liu:** Writing – original draft, Validation, Supervision, Resources, Funding acquisition, Conceptualization. **Chunlin Zhuang:** Writing – review & editing, Writing – original draft, Validation, Supervision, Resources, Methodology, Funding acquisition, Conceptualization.

Declaration of competing interest

The authors declare that they have no known competing financial interests or personal relationships that could have appeared to influence the work reported in this paper.

Acknowledgments

This work was funded by grants from the National Key R&D Program of China (No. 2021YFA1302200), National Natural Science Foundation of China (Nos. 82574241, 82022065), the Zhuoyue and Jingying Programs of Second Military Medical University.

Supplementary materials

Supplementary material associated with this article can be found, in the online version, at doi:10.1016/j.cclet.2025.112111.

References

[1] T. Kobayashi, B. Siegmund, C.Le Berre, et al., Nat. Rev. Dis. Primers 6 (2020) 74.
[2] S.C. Ng, H.Y. Shi, N. Hamidi, et al., Lancet 390 (2017) 2769–2778.
[3] H. Nakase, M. Uchino, S. Shinzaki, et al., J. Gastroenterol. 56 (2021) 489–526.
[4] S.C. Truelove, L.J. Witts, Br. Med. J. 2 (1955) 1041–1048.
[5] H.M. Khan, F. Mehmood, N. Khan, Clin. Exp. Gastroenterol. 8 (2015) 293–302.
[6] P. Wangchuk, K. Yeshi, A. Loukas, Trends Pharmacol. Sci. 45 (2024) 892–903.
[7] Q. Lu, M.F. Yang, Y.J. Liang, et al., J. Inflamm. Res. 15 (2022) 1825–1844.
[8] A. Yu, N.B. Ha, B. Shi, et al., Clin. Gastroenterol. Hepatol. 21 (2023) 3115–3124 e3113.
[9] M.R. Henn, E.J. O'Brien, L. Diao, et al., Gastroenterology 160 (2021) 115–127.e30.
[10] K. Ishikawa, S. Sugimoto, M. Oda, et al., Gastroenterology 163 (2022) 1391–1406.e24.
[11] J.V. Patankar, C. Becker, Nat. Rev. Gastroenterol. Hepatol. 17 (2020) 543–556.
[12] J. Silke, J.A. Rickard, M. Gerlic, Nat. Immunol. 16 (2015) 689–697.
[13] L. Xu, C. Zhuang, Med. Res. Rev. 43 (2023) 1974–2024.
[14] C. Chelakkot, J. Ghim, S.H. Ryu, Exp. Mol. Med. 50 (2018) 1–9.
[15] C. Guo, J. He, X. Song, et al., Pharmacol Res. 149 (2019) 104463.
[16] L.J. Xu, Y. Tu, J. Li, et al., Chin. Chem. Lett. 33 (2022) 2545–2549.
[17] L. Duprez, N. Takahashi, F. Van Hauwermeiren, et al., Immunity 35 (2011) 908–918.
[18] J. Zhu, M. Xin, C. Xu, et al., Acta Pharm. Sin. B 11 (2021) 3193–3205.
[19] L. Yin, X. Jiang, M. Wang, et al., Chin. Chem. Lett. 36 (2025) 110224.
[20] Y. Guo, M. Zhou, Z. Mu, et al., Biomed. Pharmacother. 165 (2023) 115138.
[21] M. Valipour, Eur. J. Med. Chem. 235 (2022) 114314.
[22] M.J. Niphakis, B.F. Cravatt, Cell Chem. Biol. 31 (2024) 1636–1651.
[23] J.M. Wozniak, W. Li, C.G. Parker, Trends Pharmacol. Sci. 45 (2024) 969–981.
[24] S. Wang, Y. Zhang, R. Yu, et al., J. Med. Chem. 67 (2024) 17980–17996.
[25] Y. Zou, Y. Chai, B. Du, et al., J. Med. Chem. 68 (2025) 9906–9925.
[26] B. Lomenick, R. Hao, N. Jonai, et al., Proc. Natl. Acad. Sci. U. S. A. 106 (2009) 21984–21989.
[27] Q. Huang, J. Liao, J. Li, et al., Chin. Chem. Lett. 36 (2025) 109914.
[28] Y. He, R. Guo, L. Yang, et al., Chin. Chem. Lett. 36 (2025) 110778.
[29] A. Lotfi, Z. Abroodi, M. Khazaei, Neurodegener. Dis. Manag. 14 (2024) 241–256.
[30] J. Yang, K. Wang, S. Sun, et al., Chin. Chem. Lett. 36 (2025) 110180.
[31] L. Dong, H. Du, M. Zhang, et al., Phytother. Res. 36 (2022) 2081–2094.
[32] E. Wu, W. He, C. Wu, et al., Cell Res. 33 (2023) 851–866.
[33] M. Mompeán, W. Li, J. Li, et al., Cell 173 (2018) 1244–1253.e1210.